Assessing the Freeze/Thaw States in Arctic Circle Using FengYun-3E GNOS-R: An Initial Demonstration and Analysis

Xuerui Wu, Xinqiu Ouyang, Shengli Wu, Fang Wang, and Zheng Duan

***Abstract*—In this article, we present the first demonstration of the FengYun-3E (FY3E) Global Navigation Satellite System Occultation Sounder II-Reflectometry (GNOS-R) payload's capacity to detect near-surface soil freeze/thaw (F/T) states. This study offers an initial analysis of the F/T retrieval algorithm applied to data collected from the Arctic Circle, underscoring the GNOS-R's potential to deliver long-term near-surface soil F/T products. Data for the period extending from the launch day of GNOS-R (Day of Year (DOY) 179, 2021) to DOY 270 in 2022 were analyzed using the surface reflectivity (SR) ratio factor to discriminate F/T variations. Comparisons were made with soil moisture active passive (SMAP) F/T products, serving as an auxiliary analysis. We found a strong consistency between SR ratio factor and SMAP F/T values, with the accuracy of the F/T retrieval algorithm exceeding 60%. These findings corroborate the efficacy of the GNOS-R payload aboard FY3E in monitoring F/T patterns at higher latitudes, specifically, the Arctic Circle. The outcomes of this study will be beneficial for future F/T detection efforts using spaceborne Global Navigation Satellite System-Reflectometry payloads.**

***Index Terms*—Arctic circle, freeze/thaw (F/T) retrieval, Global Navigation Satellite System Occultation Sounder II-reflectometry (GNOS-R), Global Navigation Satellite System-Reflectometry (GNSS-R), soil moisture active passive (SMAP).**

Manuscript received 12 September 2023; revised 17 October 2023; accepted 24 October 2023. Date of publication 30 October 2023; date of current version 23 November 2023. This work was supported by the National Natural Science Foundation of China under Grant 42061057 and in part by the Multi-band Satellite Navigation Intelligent Remote Sensing Technology project of the Key Laboratory Fund for Key Laboratory of Satellite Navigation Technology. *(Corresponding author: Xuerui Wu.)*

Xuerui Wu is with Shanghai Astronomical Observatory, Chinese Academy of Sciences, Shanghai 200030, China, and also with the School of Resources, Environment and Architectural Engineering, Chifeng University, Chifeng 024000, China (e-mail: xrwu@shao.ac.cn).

Xinqiu Ouyang is with Guangzhou Urban Planning & Design Survey Research Institute, Guangzhou 510060, China (e-mail: ouyxq3@mail3.sysu.edu.cn).

Shengli Wu is with the National Satellite Meteorological Center(National Centre for Space Weather), Beijing 100081, China, also with the Innovation Center for FengYun Meteorological Satellite (FYSIC), Beijing 100081, China, and also with the Key Laboratory of Radiometric Calibration and Validation for Environmental Satellites/Key Laboratory of Space Weather, CMA, Beijing 100081, China (e-mail: wusl@cma.gov.cn).

Fang Wang is with School of Architectural Engineering, North China Institute of Science and Technology, Yanjiao 065201, China (e-mail: wangfang@cttic.cn).

Zheng Duan is with the Department of Physical Geography and Ecosystem Science, Lund University, 22362 Lund, Sweden (e-mail: zheng.duan@nateko.lu.se).

Digital Object Identifier 10.1109/JSTARS.2023.3328401

I. Introduction

THE freeze/thaw (F/T) cycle, a phase change process of water and ice, occurs annually in approximately 60% of the global land near-surface soil [1], [2]. The spatiotemporal characteristics of this F/T cycle play a crucial role in various environmental processes, including vegetation growth, energy balance, water dynamics, greenhouse gas exchange, and overall ecosystem functioning. Understanding the F/T status of near-surface soil is not only a sensitive indicator of climate change but also essential for assessing soil moisture dynamics in cold regions [3], [4].

While traditional methods can accurately describe the F/T cycle at a point scale and provide ground information for validation purposes, they are limited in their applicability to large-scale and long-term trend analyses [5]. Therefore, there is a need for remote sensing techniques that can capture F/T dynamics over extensive areas and extended time periods.

Satellite remote sensing technology has proven successful in studying various environmental phenomena at regional and global scales. The principle on how remote sensing can be used to monitor F/T dynamics is briefly described as follows. The dielectric constant of liquid water (with a relative dielectric constant of 81) significantly differs from that of ice (with a relative dielectric constant of about 3–4). As the soil undergoes melting, the phase transition of ice to liquid water increases the soil's dielectric constant. Consequently, this leads to an increase in soil reflectivity or a decrease in soil emissivity [6]. Notably, the low-frequency band ($<$10 GHz) of microwave remote sensing exhibits high sensitivity to water phase transitions, providing a theoretical foundation for F/T inversion using passive microwave remote sensing technology.

In recent years, Global Navigation Satellite System-Reflectometry (GNSS-R) has gained attention as a new method of remote sensing operating at L-band. GNSS-R utilizes reflected signals from navigation systems to monitor various geophysical parameters [7]. One of the promising applications of GNSS-R is the detection of near-surface soil freezing and thawing characteristics [8]. Researchers have explored the effectiveness of GNSS-R technology in monitoring soil F/T characteristics by employing microwave scattering models, global positioning system (GPS) multipath models, and GPS bistatic radar equation models. They have verified the potential of GNSS-Interference Reflectometry (GPS-IR) technology for monitoring

soil F/T characteristics, supported by correlation analyses using International GNSS Services station data [9].

The concept of GNSS-R was even extended to the malfunctioning soil moisture active passive (SMAP) radar. Researchers successfully collected GPS L2C signals using a special data processing method, known as SMAP-Reflectometry (SMAP-R), by tuning the SMAP radar receiver bandwidth to 1227.45 MHz [10]. SMAP-R demonstrated the potential to quantify changes in high-latitude soil F/T states at kilometer-scale resolution, as evidenced by a 10-dB seasonal difference in the signal-to-noise ratio observed in boreal wetland observations [10]. Similarly, TechDemoSat-1 (TDS-1) data have been analyzed and compared with SMAP F/T data, showing a large seasonal cycle in calibrated reflectivity that aligns effectively with SMAP F/T data [11], [12].

In specific regions like the Qinghai–Tibet Plateau and South America, researchers have utilized Cyclone Global Navigation Satellite System (CYGNSS) and SMAP data to monitor near-surface F/T characteristics and analyze the impact of snow depth [13], [14]. Results have demonstrated the effectiveness of CYGNSS in monitoring surface soil F/T status. In addition, the CYGNSS mission has been employed in three high-altitude target areas (the Tibet Plateau, the Andes, and the Rocky Mountains) to calculate the number of frozen and thawed months per year, yielding successful outcomes [15], [16].

In this study, we focus on the application of the FengYun-3E (FY-3E) satellite's Global Navigation Satellite System Occultation Sounder (GNOS-II) payload to study the F/T state of the Arctic Circle for the first time. Launched on July 10, 2021, GNOS-II consists of eight reflection channels, capable of receiving signals from GPS, Beidou Navigation System (BDS), and Galileo navigation satellites simultaneously. While GNOS-R has been utilized for studying ocean state parameters, soil moisture, and sea ice thickness, its application in studying surface F/T states is relatively unexplored [17], [18], [19], [20]. This article employs GNOS-R data from July 10, 2021, to September 27, 2022, to investigate the F/T state of the Arctic Circle.

The rest of this article is organized as follows. Section II describes the datasets used in this study. Section III presents the theoretical fundamentals underlying the GNOS-R methodology. Section IV outlines the methodology employed and presents the results of the F/T state analysis. Finally, Section V concludes this article and offers suggestions for future research directions.

II. Datasets

A. Study Area

The focused area for this study is the Arctic Circle, defined as an imaginary circle with a latitude of 66°34′ N. It serves as the boundary between the northern cold zone and the northern temperate zone and is complementary to the ecliptic angle (the latitude value of the Tropic of Cancer). The Arctic climate is characterized by long cold winters and short cool summers, with diverse climate changes. Winter temperatures average around −20 °C, reaching as low as −33° in many places. In summer, temperatures range from −10 to 10 °C. In 2022, the maximum temperature in the Arctic Circle reached 38 °C. Due to the extreme cold, the Arctic Circle has limited biological species diversity. The corresponding land cover and land use map for the Arctic Circle are presented in Fig. 1, which is calculated from MODIS data of Year 2019 [21].

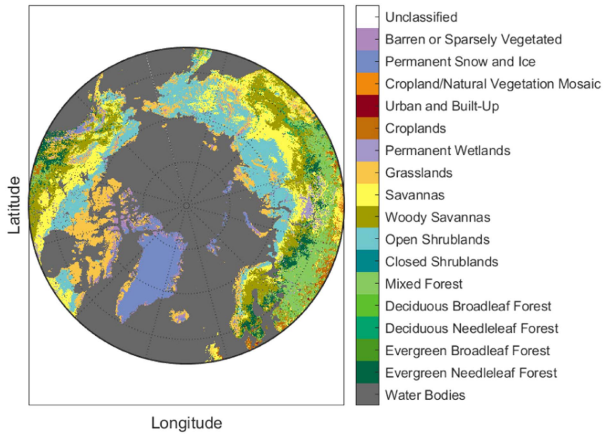

Fig. 1. Land cover and land use map in the Arctic Circle.

B. FengYun-3E GNOS-R

The FY-3E satellite is part of the FengYun satellite family and is the first early morning orbit satellite in the series. It carries a total of 11 payloads, including the GNOS-II payload, which combines GNSS-Radio Occultation and GNSS-R capabilities. In this context, the specific payload used for GNSS-R is referred to as GNOS-R. It is worth noting that future FY-3 satellites, such as FY-3F, FY-3G, and FY-3H, are also scheduled to carry GNOS-R payloads. GNOS-R has the capability to receive signals from multiple global navigation systems simultaneously, including GPS, BDS, and Galileo. Specifically, the GNOS-R sensor can receive GPS L1 C/A, BDS B1I, and GAL E1B signals. This enables the delivery of multi-GNSS reflection products to users. Unlike NASA's CYGNSS mission, which focuses on cyclone monitoring, GNOS-R has global coverage due to its orbit inclination of 98.8°. This global coverage capability makes it suitable for the potential detection of surface soil F/T status in the Arctic Circle. By utilizing GNOS-R data, it is possible to study the F/T state of the surface in the Arctic Circle, taking advantage of its wide coverage area. Here, the Level 1 (L1) data of GNOS-R are employed, while data for the period extending from the launch day of GNOS-R (Day of Year (DOY) 179, 2021) to DOY 270 in 2022 were analyzed.

C. Soil Moisture Active Passive

The SMAP satellite was launched by NASA on January 31, 2015. It is the second satellite dedicated to soil moisture observation, following the SMOS satellite launched by the European Space Agency [22]. SMAP is equipped with two instruments: an active L-band radar sensor and a passive L-band microwave radiometer sensor. These instruments are used to observe soil moisture and determine the F/T state of the same area. SMAP provides a range of data products, including 15 major data products. The L1 data products consist of corrected radar backscatter cross section and radiometer brightness temperature data. The Level 2 (L2) data products are soil moisture products obtained

from the L1 data products through inversion algorithms that utilize auxiliary data. The Level 3 (L3) products combine daily L2 soil moisture products with F/T data. Finally, the Level 4 products are derived data products aimed at effectively addressing specific scientific problems.

SMAP's data products offer valuable information about soil moisture and the F/T state, providing insights into the dynamics of the earth's surface. These data products are derived from the combination of radar and radiometer measurements, and they play a crucial role in various scientific applications and research related to soil moisture and F/T processes. Here, we employ the L3 F/T data of SMAP to work as ancillary data for analysis. The spatial resolution of these data is 36 km, while the time periods of SMAP data just cover the ones of GNOS-R.

III. Theoretical Fundamentals

A. Dielectric Constant Model

The dielectric constant of soil is influenced by various factors, including soil properties (such as texture, organic matter content, and salinity), water content, temperature, and frequency. Among these factors, temperature variations play a significant role in the transformation of soil F/T processes. The F/T process is essentially a phase change of liquid water within the soil. During the soil freezing process, not all the water in the soil freezes. Some water remains unfrozen due to capillary action and adsorption on the soil particles' surfaces. This unfrozen water content gradually decreases as the temperature decreases and vice versa. Accurately estimating the unfrozen water content is crucial for developing a dielectric model for frozen or thawed soil.

Currently, the dielectric model for F/T soil is an extension of the Dobson model [23]. The Dobson model is a well-known dielectric model that describes the relationship between soil moisture content and the dielectric constant of unfrozen soil. The extension of this model, i.e., Zhang–Zhao model, incorporates the effects of frozen water content and temperature on the dielectric constant by considering the unfrozen water content and temperature; the dielectric constant model for F/T soil can provide estimates of the dielectric properties of soil under different F/T conditions [24], [25]. This model is essential for understanding and quantifying the electromagnetic properties of frozen or thawed soil, which is crucial for various applications, including remote sensing, soil moisture retrieval, and environmental studies in cold regions

$$\varepsilon_m'^{a} = \begin{cases} 1+\frac{\rho_b}{\rho_s}(\varepsilon_s'^{a}-1)+\theta_{vu}^{\beta'}\varepsilon_{fw}'^{\alpha}-\theta_{vu}, & T>0^{\circ}\mathrm{C} \\ 1+\frac{\rho_b}{\rho_s}(\varepsilon_s'^{a}-1)+\theta_{vu}^{\beta'}\varepsilon_{fw}'^{\alpha}-\theta_{vu}+\theta_{vi}^{\beta'}\varepsilon_i'^{\alpha}-\theta_{vi}, & T\le 0^{\circ}\mathrm{C} \end{cases} \tag{1}$$

$$\varepsilon_m''^{a} = \theta_{vu}^{\beta''}\varepsilon_{fw}''^{\alpha}. \tag{2}$$

ε' and ε'' are the real part and the imaginary part of the dielectric constant, respectively, and the subscripts of m, s, fw, and i represent the moist soil, mineral particles, liquid water (containing free and bound water), and ice, respectively. Subscripts u and i represent volume proportion unfrozen water and ice, respectively. α is the shape factor. β' and β'' are empirical parameters related to soil texture to express the effect of bound water; the parameterization scheme for unfrozen water content represents it as a function of temperature (absolute difference from freezing point), initial (maximum) water content, and minimum unfrozen water content. The relationship between the real part and the imaginary part of the dielectric constant with the soil temperature is shown in Fig. 1. We can see that there is an apparent change as the soil change from frozen state to the thaw state.

B. Surface Reflectivity (SR) at Long-Range (LR) Polarization

Utilizing the dielectric constants of both frozen and thawed soil, we can derive the associated SR. It is widely acknowledged that coherent scattering reflectivity plays a pivotal role in discerning the frozen or thawed state of surface soil. To quantify this phenomenon, we employ the subsequent equations to compute the surface coherent reflectivity. Specifically, we consider the Fresnel reflectivity for both vertical and horizontal polarizations, as outlined below

$$r_h = \frac{\cos\theta - \sqrt{\varepsilon - \sin\theta^2}}{\cos\theta + \sqrt{\varepsilon - \sin\theta^2}} \tag{3}$$

$$r_v = \frac{\varepsilon\cos\theta - \sqrt{\varepsilon - \sin\theta^2}}{\varepsilon\cos\theta + \sqrt{\varepsilon - \sin\theta^2}} \tag{4}$$

where θ is the incidence angle, ε is the complex dielectric constant, and the subscripts h and v demonstrate the polarization state.

The investigation of SR for GNSS-R studies often centers around LR polarization. By utilizing linear combinations of the vertical and horizontal polarization Fresnel reflectivity, we can derive the equations that govern the SR for LR polarizations, as follows [22]:

$$\Gamma_{\mathrm{LR}} = \frac{(\varepsilon-1)^2\cos\theta^2\left(\varepsilon-\sin\theta^2\right)}{\left(\varepsilon\cos\theta+\sqrt{\varepsilon-\sin\theta^2}\right)\left(\cos\theta+\sqrt{\varepsilon-\sin\theta^2}\right)^2}. \tag{5}$$

C. LAGRS-FT Model for Delay Doppler Mapping Waveform

The LAGRS model, standing for Long-Range Advanced GNSS-R Simulator for Delay Doppler Mapping (DDM), serves as an extensive spaceborne GNSS-R observables simulator. This model enables the computation and simulation of DDMs, which constitute the ultimate outputs of spaceborne GNSS-R observables [26], [27]. Notably, the LAGRS model was originally designed to calculate various land surface geophysical parameters, encompassing soil, vegetation, and flood conditions. In addition, a dedicated module is incorporated into LAGRS for the specific purpose of detecting surface soil F/T states [28].

A distinguishing feature of this F/T detection module, in comparison to other components within LAGRS, lies in the formulation employed for calculating dielectric constants and reflectivity. The methodologies for frozen and thawed soil are elaborated upon in Sections III-A and III-B, respectively. A

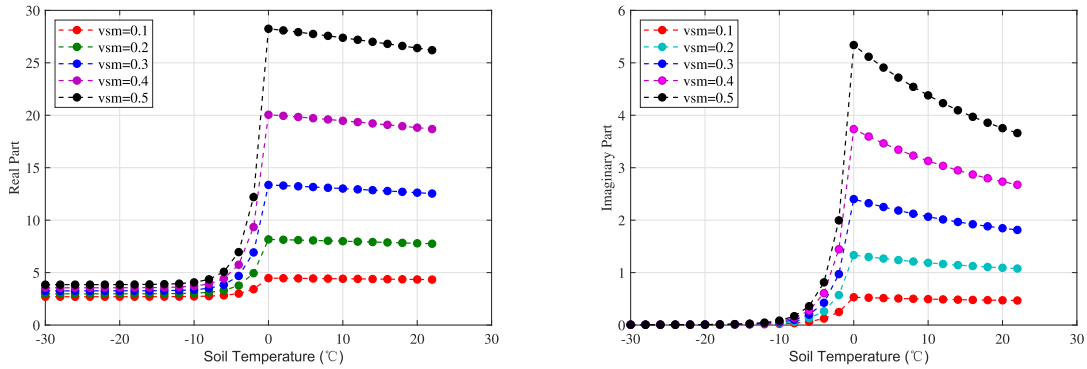

Fig. 2. Dielectric constant of real part (left figure) and imaginary part (right figure) versus the soil temperature at different soil moisture content for GPS L1 frequency band.

schematic representation of the theoretical foundations governing soil F/T detection is depicted in Fig. 2. Leveraging information regarding soil texture, moisture content, temperature, bulk density, and shape factor, we can deduce the physical and dielectric properties of the soil. Subsequently, the model, as detailed in Section III-A, facilitates the determination of dielectric constants for both frozen and thawed soil.

By incorporating parameters such as transmitter and receiver velocities and positions, the observation geometry can be ascertained. This, in turn, enables the computation of the specular incidence angle. As a result, the SR for LR polarization can be obtained using (5). The LAGRS F/T model calculates DDM observables, which are subsequently employed to differentiate between near-surface frozen and thawed states. The flowchart for the theoretical fundamentals of soil F/T detection is presented in Fig. 3.

IV. Results and Discussion

A. SR Estimation

The original observation of GNSS-R is DDM, which is used to retrieve the final geophysical parameters. The DDM generated by the GNOS-R receiver is nonuniform in comparison to the standard uniform DDM from the TDS-1 and CYGNSS L1 products; the purpose of this design is to gain additional sampling around the specular point. In order to do the following discrimination for surface soil F/T detection, we will employ the peak values of DDM. While we call this value as SR, its equation for the final calculation is like the following [19]:

$$\Gamma(\theta) = \frac{(R_r + R_t)^2 (P_{\mathrm{DDM}} - N)}{F R_t^2 R_r^2 4\pi} \tag{6}$$

where Γ is the SR, R_r and R_t are the distances from the specular points to the receiver and the transmitter, respectively, P_{DDM} is the peak DDM power, N refers to noise, and F is the DDM bistatic radar cross section factor, and it can be defined as

$$F = \frac{\lambda^2 P_t G_t G_r}{(4\pi)^3 R_t^2 R_r^2}. \tag{7}$$

B. Definition of Discriminant Algorithms

A seasonal threshold algorithm (STA) is developed and employed for the retrieving F/T surface state from CYGNSS measurements [15]. The STA algorithm is to estimate the present SR ($\mathrm{SR_{pre}}$) in the fixed time series with the SR at the frozen ($\mathrm{SR_{min}}$) and thawed ($\mathrm{SR_{max}}$) states, while the maximum and minimum SRs in the frozen state and thawed states are set as the reference data. We will call this definition as SR ratio factor

$$\Delta \mathrm{SR}(t) = \frac{\mathrm{SR_{pre}} - \mathrm{SR_{min}}}{\mathrm{SR_{max}} - \mathrm{SR_{min}}}. \tag{8}$$

During our calculations, we take the average of the top five highest reflectivity values within the time series as $\mathrm{SR_{max}}$, while the average of the five lowest reflectivity values within the time series as $\mathrm{SR_{min}}$. With this algorithm, we can calculate the frozen or thawed state. $\mathrm{SR_{min}}$ and $\mathrm{SR_{max}}$ are presented in Fig. 4(a) and (b), and the corresponding threshold for the final discriminant is presented in Fig. 4(c). It should be mentioned that apparent SR difference can be seen from Fig. 4(a) and (b) that the SR in summer [see Fig. 4(a)] is larger than that in winter [see Fig. 4(b)], which is due to the higher specular reflectivity in summer.

C. Discriminant Results

Based on the land cover and land use data provided in the preceding section, our analysis focuses on classifying the land surface within the Arctic Circle into five distinct types: barren (exposing bare soil), LowVeg (with low vegetation covering the soil), Forest (encompassing forested areas), snow/ice, and water surfaces. However, for the subsequent analysis, we concentrate solely on three land surface types, i.e., Barren, LowVeg, and Forest, because these kinds of land cover types are more related to the soil F/T status. Fig. 5 shows the SR during the studied time periods for these three types of land surfaces.

An evident cyclic pattern in SR becomes apparent from Fig. 5, relating to the three mentioned land surface types. As anticipated, generally lower reflectivity values associated with lower permittivity have been obtained during winter months. Conversely, higher reflectivity values have predominantly been observed in areas with a greater proportion of thawed pixels (higher permittivity). As the transition occurs from summer to winter or vice versa, SR values progressively shift from higher to lower values and vice versa. This cyclic SR variation for GNSS-R aligns with the phenomenon demonstrated in TDS-1's pioneering work [11], the initial paper illustrating the feasibility

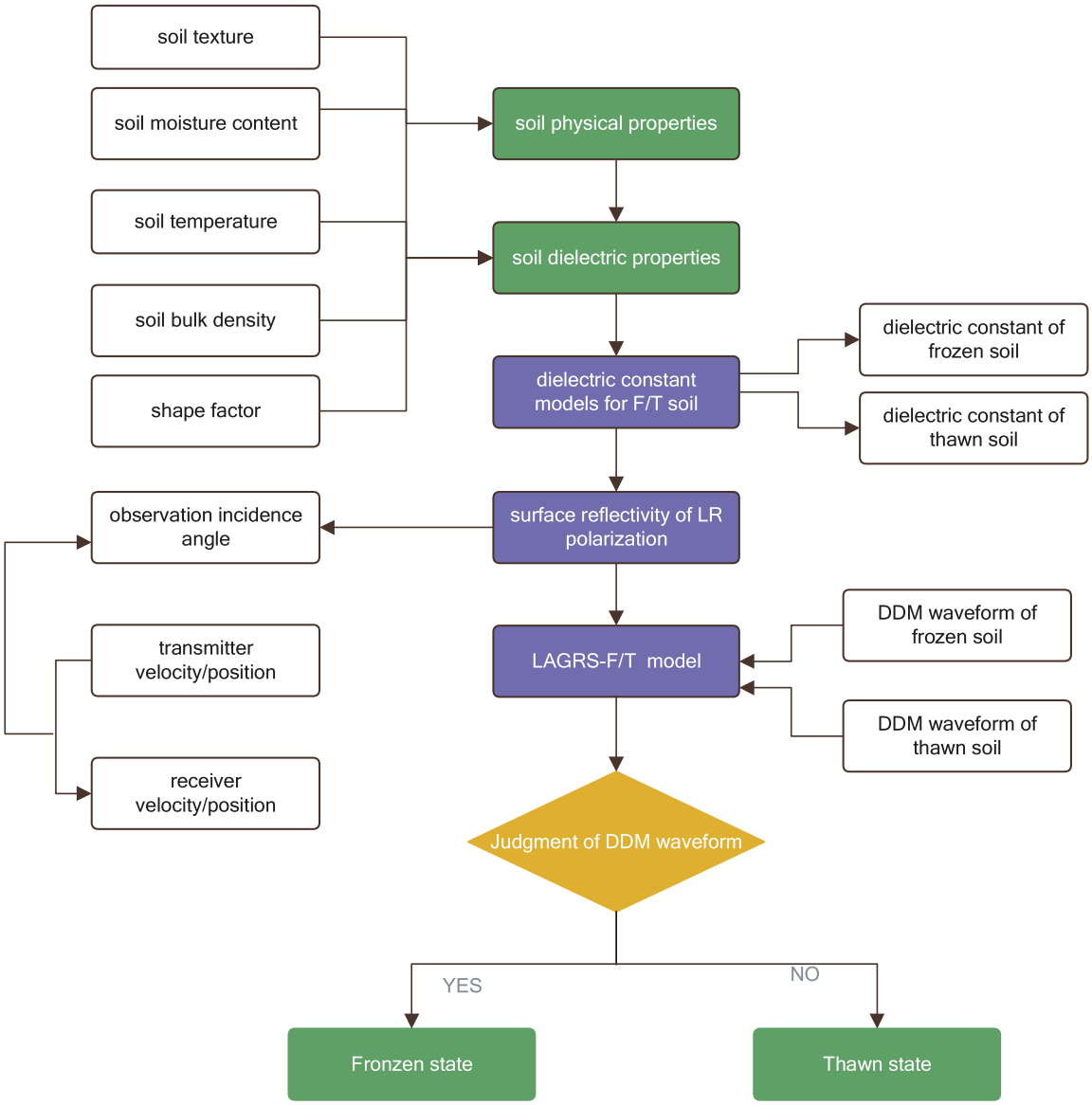

Fig. 3. Flowchart for the theoretical fundamentals of soil F/T detection. The blue boxes indicate the models employed for the soil F/T detection, while the green ones are the main features of the fundamentals and the ones without colors are inputs (left part) and outputs (right part) of the models. Here, DDM is short for delay Doppler map, which is the final observable of GNOS-R payload.

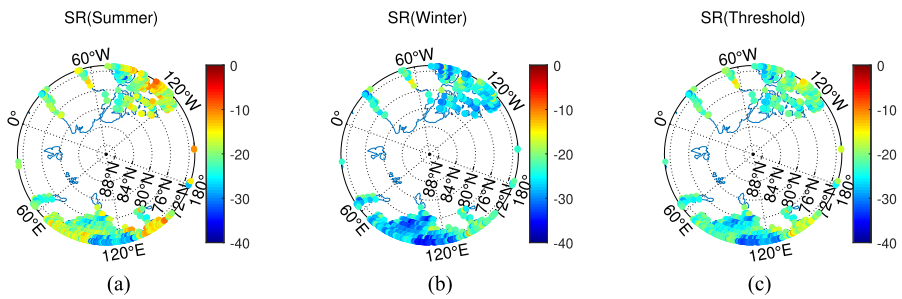

Fig. 4. SR at (a) summer, (b) winter, and (c) the final threshold.

TABLE I
NUMBER OF FROZEN PIXELS AND EFFECTIVE PIXELS, DATA FOR THE PERIOD EXTENDING FROM THE LAUNCH DAY OF GNOS-R (DOY 179, 2021) TO DOY 270 IN 2022

Time period (DOY)	317–330	331–344	345	359 to 21	22–35	36–49	50–63	64–77	78–91	92–105
	Year 2021			Year 2021 to 2022	Year 2022					
No. of Frozen pixels	10529	12116	14408	18208	16232	15862	13569	12010	8948	8274
No. of effective pixels	17202	18481	22792	22997	20412	19957	18462	15851	12206	11592

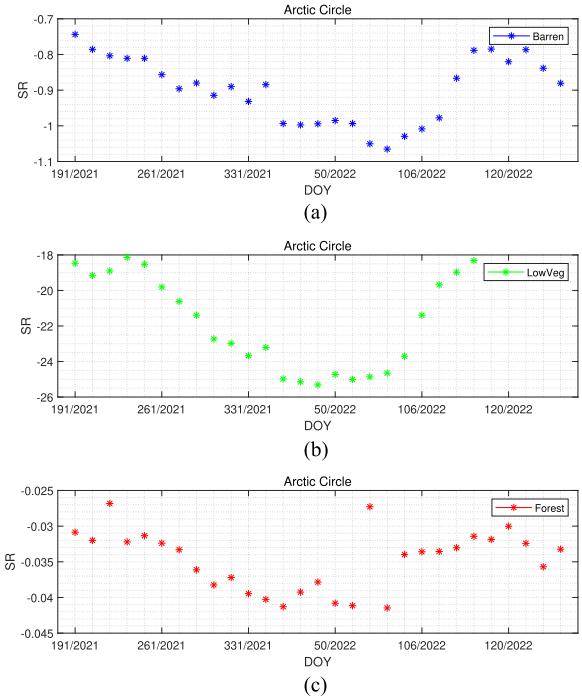

Fig. 5. SR data for three types of land surfaces in Arctic Circle. (a) Barren. (b) LowVeg. (c) Forest.

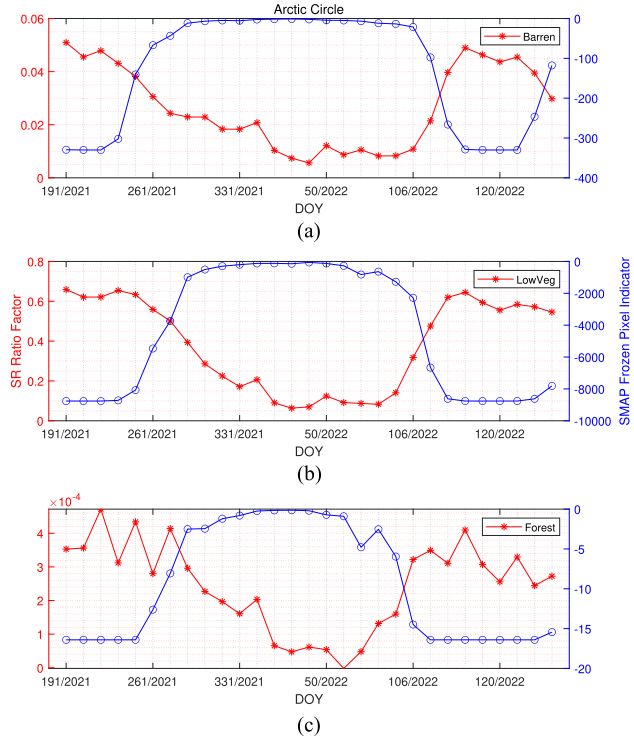

Fig. 6. SR ratio factors (left Y-axis) and the SMAP F/T values (right Y-axis) for three types of land surfaces [(a) barren, (b) LowVeg, and (c) Forest] in Arctic Circle during the periods of July 10, 2021 to July 10, 2022. The DOY is used to represent the date during the studied period in the X-axis.

of utilizing spaceborne GNSS-R for detecting surface soil F/T conditions.

Fig. 6 illustrates the relationship between SR ratio factors and SMAP F/T values. Remarkably, we observe an inverse periodic trend between the SR ratio factors employed in generating the surface soil F/T discriminant map and the SMAP-derived F/T values. The latter values, extracted from SMAP data, serve as indicators for surface soil F/T conditions. This coherence between the SR ratio factors and SMAP F/T values validates the use of SR ratio factors as reliable discriminant indicators for surface soil F/T conditions. The conclusive results are depicted in Figs. 7 and 8, with one representative subfigure highlighted, focusing on the period from DOY 331 to 344 in the year 2021. The alignment between these figures is notably good, confirming their consistency.

In addition, we delve into quantitative analysis, particularly for colder days within two distinct periods: DOY 317–359 in the year 2021 and DOY 345 in the year 2022. Fig. 9 presents the results of this analysis, showcasing correct discrimination

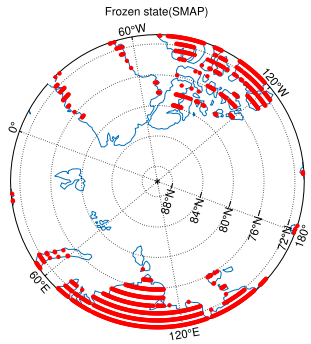

Fig. 7. Surface soil frozen state calculated from SMAP for the period DOY 331–344 in the year 2021, while the red point means the frozen pixel.

percentages. Impressively, correct discrimination percentages exceed 60%, with a significant portion surpassing the 70% mark.

To further illuminate our findings, we provide Table I, offering the corresponding counts of frozen pixels and effective pixels

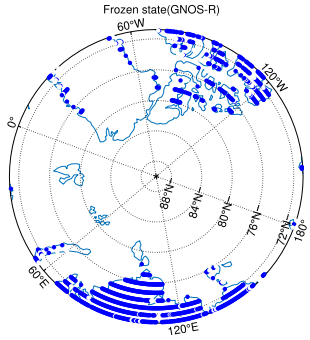

Fig. 8. Surface soil frozen state calculated from F3E GNOS-R for the period DOY 331–344 in the year 2021. The blue points mean the frozen pixels calculated from GNOS-R data.

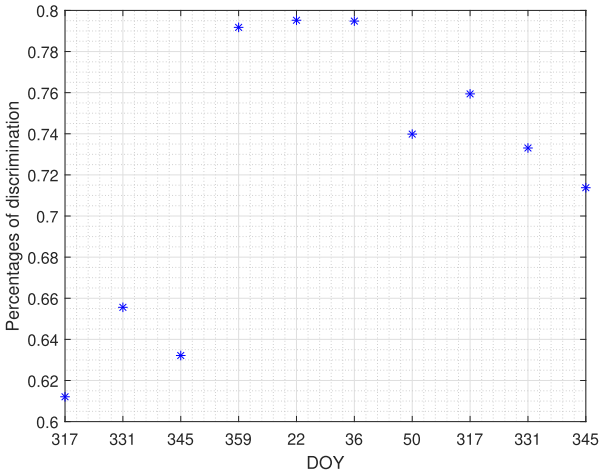

Fig. 9. Quantitative analysis for the colder days during the periods (between DOY 317 and 359 in the year 2021 and DOY 345 in the year 2022).

during the aforementioned periods (DOY 317–359 in the year 2021 and DOY 345 in the year 2022). Here, the number of frozen pixels is calculated by adding up all the frozen pixels during that specified time period. Meanwhile, the number of corresponding effective pixels refers to all the pixels that are taken into account for the calculation. This table succinctly encapsulates the data essential to our quantitative assessment.

V. Conclusion

The determination of near-surface soil F/T states holds great significance, serving as a vital and sensitive parameter for comprehending climate change dynamics and hydrological processes. In this context, the emerging spaceborne GNSS-R technique offers a promising augmentation to conventional remote sensing methodologies. Our study focused on F3E GNOS-R data collected from DOY 179 in the year 2021 to DOY 270 in the year 2022, encompassing the Arctic Circle. This region is strategically chosen due to the distinct and periodic F/T alterations occurring within the surface soil during this time frame.

Leveraging auxiliary SMAP F/T data, we carried out comprehensive analyses. An essential aspect of our study involved the calculation of an SR ratio factor, aiding in the assessment of frozen pixels across the Arctic Circle. The noteworthy coherence achieved between the SR ratio factor derived from GNOS-R data and SMAP F/T values underscores the reliability of our approach. Specifically, during the colder periods spanning DOY 317–359 in the year 2021 and DOY 345 in the year 2022, our method yielded an impressive result: nearly 70% of the correct discrimination percentages exceeded 70%.

It is important to note that although the discriminant algorithm presented in this article has yielded promising results, it does not account for the snow layer's effects, which has not considered for almost all of the present spaceborne GNSS-R, such as TDS-1 and CYGNSS. Specifically, a damp snow layer poses a unique challenge for identifying thawing soil conditions. With its low reflectivity, it can be easily mistaken for frozen ground. However, during the melting process, relying solely on reflectivity values may lead to an inaccurate assessment of snow melt. To overcome this challenge, it is essential to incorporate appropriate auxiliary data to detect melting snow accurately. This approach can help minimize errors and provide more reliable information about soil thaw cycles.

Our study successfully demonstrates the substantial potential of GNOS-R in detecting surface F/T conditions. The ability of GNOS-R to cover global regions enhances its utility for this purpose, particularly in higher latitude areas—a capability not shared by CYGNSS due to its pan-tropical coverage. The future deployment of GNOS-R payloads on the upcoming FengYun series satellites holds promise for achieving higher spatial and temporal resolutions in near-surface F/T products. As the subsequent polarization GNOS-R payloads are launched on FengYun series satellites, new polarization information will provide great potential for the development of discriminant algorithms that rely on polarization in the form of RR, LR, and other linear–circular combinations. This advancement will considerably amplify the practical applications of spaceborne GNSS-R technology, and the near-surface F/T products based on the algorithm in this article will also provide commercial products for global climate and meteorological research. It will be a valuable addition to the current traditional microwave radiometer and SAR technology.

References

[1] C. Godde, D. Mason-D'Croz, D. Mayberry, P. K. Thornton, and M. Herrero, "Impacts of climate change on the livestock food supply chain; A review of the evidence," *Glob. Food Secur.*, vol. 28, 2021, Art. no. 100488.

[2] L. Hu et al., "A twenty-year dataset of soil moisture and vegetation optical depth from AMSR-E/2 measurements using the multi-channel collaborative algorithm," *Remote Sens. Environ.*, vol. 292, 2023, Art. no. 113595.

[3] T. Zhao, L. Zhang, L. Jiang, S. Zhao, L. Chai, and R. Jin, "A new soil freeze/thaw discriminant algorithm using AMSR-E passive microwave imagery," *Hydrological Processes*, vol. 25, pp. 1704–1716, 2011.

[4] T. Zhao et al., "Estimation of high-resolution near-surface freeze/thaw state by the integration of microwave and thermal infrared remote sensing data on the Tibetan plateau," *Earth Space Sci.*, vol. 4, no. 8, pp. 472–484, Aug. 2017.

[5] Y. Qiu, H. K. Lappalainen, T. Che, S. Sandven, and T. Zhao, "Observations and geophysical value-added datasets for cold high mountain and polar regions," *Big Earth Data*, vol. 6, pp. 381–384, 2022.

[6] F. T. Ulaby, R. K. Moore, and A. K. Fung, *Microwave Remote Sensing Active and Passive-Volume II: Radar Remote Sensing and Surface Scattering and Enission Theory*. Norwood, MA, USA: Artech House, 1982.
[7] M. Martin-Neira, "A passive reflectometry and interferometry system (PARIS): Application to ocean altimetry," *ESA J.*, vol. 17, no. 4, pp. 331–355, 1993.
[8] X. Wu and S. Jin, "Can we monitor the bare soil freeze-thaw process using GNSS-R? A simulation study," in *Proc. SPIE*, vol. 9264, 2014, Art. no. 92640I.
[9] W. Xuerui, J. Shuanggen, and C. Liang, "Monitoring bare soil freeze–thaw process using GPS-interferometric reflectometry: Simulation and validation," *Remote Sens.*, vol. 10, no. 1, 2017, Art. no. 14.
[10] C. Chew et al., "SMAP radar receiver measures land surface freeze/thaw state through capture of forward-scattered L-band signals," *Remote Sens. Environ. Interdiscipl. J.*, vol. 198, pp. 333–344, 2017.
[11] D. Comite, L. Cenci, A. Colliander, and N. Pierdicca, "Monitoring freeze-thaw state by means of GNSS reflectometry: An analysis of TechDemoSat-1 data," *IEEE J. Sel. Topics Appl. Earth Observ. Remote Sens.*, vol. 13, pp. 2996–3005, 2020.
[12] K. Rautiainen, D. Comite, J. Cohen, E. Cardellach, M. Unwin, and N. Pierdicca, "Freeze–thaw detection over high-latitude regions by means of GNSS-R data," *IEEE Trans. Geosci. Remote Sens.*, vol. 60, 2022, Art. no. 4302713.
[13] X. Wu et al., "First measurement of soil freeze/thaw cycles in the tibetan plateau using CYGNSS GNSS-R data," *Remote Sens.*, vol. 12, no. 15, 2020, Art. no. 2361.
[14] W. Ma, L. Huang, X. Wu, S. Jin, W. Bai, and X. Li, "Evaluation of CYGNSS observations for snow properties, a case study in tibetan plateau, China," *Remote Sens.*, vol. 14, no. 15, 2022, Art. no. 3772.
[15] H. Carreno-Luengo and C. S. Ruf, "Retrieving freeze/thaw surface state from CYGNSS measurements," *IEEE Trans. Geosci. Remote Sens.*, vol. 60, 2021, Art no. 4302313.
[16] H. Carreno-Luengo and C. S. Ruf, "Mapping freezing and thawing surface state periods with the CYGNSS based F/T seasonal threshold algorithm," *IEEE J. Sel. Topics Appl. Earth Observ. Remote Sens.*, vol. 15, pp. 9943–9952, 2022.
[17] G. Yang et al., "FY3E GNOS II GNSS reflectometry: Mission review and first results," *Remote Sens.*, vol. 14, no. 4, 2022, Art. no. 988.
[18] F. Huang et al., "Spaceborne GNSS reflectometry with galileo signals on FY-3E/GNOS-II: Measurements, calibration, and wind speed retrieval," *IEEE Geosci. Remote Sens. Lett.*, vol. 20, 2023, Art. no. 3501505.
[19] G. Yang et al., "An illustration of FY-3E GNOS-R for global soil moisture monitoring," *Sensors*, vol. 23, no. 13, 2023, Art. no. 5825.
[20] C. Yin et al., "Sea ice detection with FY3E GNOS II GNSS reflectometry," in *Proc. IEEE Spec. Meeting Reflectometry GNSS Signals Opportunity*, 2021, pp. 36–38.
[21] L. M. See and S. Fritz, "A method to compare and improve land cover datasets: Application to the GLC-2000 and MODIS land cover products," *IEEE Trans. Geosci. Remote Sens.*, vol. 44, no. 7, pp. 1740–1746, Jul. 2006.
[22] V. U. Zavorotny and A. G. Voronovich, "Scattering of GPS signals from the ocean with wind remote sensing application," *IEEE Trans. Geosci. Remote Sens.*, vol. 38, no. 2, pp. 951–964, Mar. 2000.
[23] M. C. Dobson, F. T. Ulaby, M. T. Hallikainen, and M. A. El-rayes, "Microwave dielectric behavior of wet soil—Part II: Dielectric mixing models," *IEEE Trans. Geosci. Remote Sens.*, vol. GE-23, no. 1, pp. 35–46, Jan. 1985.
[24] L. Zhang, T. Zhao, L. Jiang, and S. Zhao, "Estimate of phase transition water content in freeze–thaw process using microwave radiometer," *IEEE Trans. Geosci. Remote Sens.*, vol. 48, no. 12, pp. 4248–4255, Dec. 2010.
[25] S. Wu, T. Zhao, J. Pan, H. Xue, L. Zhao, and J. Shi, "Improvement in modeling soil dielectric properties during freeze-thaw transitions," *IEEE Geosci. Remote Sens. Lett.*, vol. 19, 2022, Art no. 2001005.
[26] X. Wu and F. Wang, "LAGRS-Veg: A spaceborne vegetation simulator for full polarization GNSS-reflectometry," *GPS Solutions*, vol. 27, no. 3, 2023, Art. no. 107.
[27] X. Wu and J. Xia, "A land surface GNSS reflection simulator (LAGRS) FORFY-3E GNSS-R payload: Part I. Bare soil simulator," in *Proc. IEEE Spec. Meeting Reflectometry GNSS Signals Opportunity*, 2021, pp. 90–92.
[28] X. Wu, S. Jin, and X. Ouyang, "A full-polarization GNSS-R delay-doppler-map (DDM) simulator for bare soil freeze/thaw process detection," *Geosci. Lett.*, vol. 7, 2020, Art. no. 4.

Xuerui Wu received the Ph.D. degree in land surface theoretical modelling and applications of GNSS-Reflectometry from Dalian Maritime University, Dalian, China, in 2012.

From 2013 to 2014, she was the Postdoctoral Researcher with Shanghai Astronomical Observatory, Chinese Academy of Sciences, Shanghai, China, where she is currently an Associate Professor. Her Ph.D. research was focused on Global Navigation Satellite System-Reflectometry (GNSS-R) land surface scattering models. Her research interests include GNSS-R and hydrology.

Xinqiu Ouyang received the B.Ec. degree in finance and the M.Sc. degree in cartography and geography information system from Sun Yat-sen University, Guangzhou, China, in 2019 and 2022, respectively.

She is currently an Assistant Engineer with the Geographic Information Center of Guangzhou Urban Planning and Design Survey Research Institute, Guangzhou. Her research interests include global change and extreme weather, urban big data, regional economics, remote sensing, and geographic information system applications.

Shengli Wu received the B.S. degree in environmental science from Peking University, Beijing, China, in 2001, and the Ph.D. degree in cartography and geography information system from the Institute of Remote Sensing Application, Chinese Academy of Sciences, Beijing, China, in 2006.

He is currently a Research Scientist with the National Satellite Meteorological Center, China Meteorological Center, Beijing. He takes on the position of the Principal Investigator of the FengYun-3C/3D/3F/3G Microwave Radiation Imager instrument, leading the ground Cal/Val and data preprocessing work. He is also the Co-Chair of Global Spacebased Inter-Calibration System by the World Meteorological Organization and the Coordination Group for Meteorological Satellites. His main research interests include microwave radiometer calibration and snow and ice parameter retrieval.

Fang Wang received the Ph.D. degree in microwave vegetation scattering modelling from Beijing Normal University, Beijing, China.

She is currently an Associate Professor with the China Transport Telecommunications and Information Center, Beijing. She has developed a coherent vegetation model based on the commonly used RT model. Her research interests include microwave radiative transfer model of vegetation.

Zheng Duan received the M.S. degree in cartography and geographic information systems from the University of Chinese Academy of Sciences, Beijing, China, in 2010, and the Ph.D. degree in remote sensing and hydrological model from the Delft University of Technology, Delft, The Netherlands, in 2014.

He was a Scientific Consultant with several institutes including UNESCO Institute for Water Education, Delft. He is currently an Associate Professor with the Department of Physical Geography and Ecosystem Science, Lund University, Lund, Sweden. His research interests include integration of remote sensing in hydrological model and water balance studies of lakes and catchments, evapotranspiration, and open water evaporation estimation.